LANGMUIR

pubs.acs.org/Langmuir Tutorial

Effect of Camera Parallax Angle on the Accuracy of Static Contact Angle Measurements

Published as part of Langmuir virtual special issue "2023 Pioneers in Applied and Fundamental Interfacial Chemistry: Nicholas D. Spencer".

Owen M. Johnson and Filippo Mangolini*

Cite This: *Langmuir* 2024, 40, 5090–5097 Read Online

ACCESS | Metrics & More | Article Recommendations | Supporting Information

ABSTRACT: Measuring the contact angle at the solid/liquid/vapor triple point in sessile drop experiments is one of the most popular and simple ways to quantify the wettability of surfaces and determine the surface free energy. Despite decades of technical advancements in contact angle measurements, which allowed for improving the precision of sessile drop measurements below ±1°, an often overlooked source of experimental error in these measurements originates from the camera's parallax angle (PA) − the angle between the camera optical axis and the sample stage surface. Here, we quantified the systematic errors in the measurement of contact angles due to the acquisition of drop images at finite PA values by simulating sessile drop experiments in which synthetic drops were created using the Young−Laplace equation. The absolute contact angle error induced by imaging drops at nonzero PAs was found to increase as the true contact angle (TCA) deviates from 90° and resulted in an overestimation (underestimation) of the contact angle for drops having TCAs lower (higher) than 90°. The computed absolute contact angle error reaches values as high as −20° (+12.2°) for drops having a TCA of 175° (5°) when imaged with a PA of 10°, thus indicating the importance of considering the PA when accurately quantifying contact angles in sessile drop experiments. The shape and, by extension, volume of the sessile drop was also found to affect the magnitude of the absolute contact angle error as sessile drops with higher apex curvatures exhibited lower absolute error than those with lower curvatures at any given PA. The outcomes of this work provide guidelines for minimizing systematic errors in sessile drop measurements due to the collection of drop images at nonzero PAs.

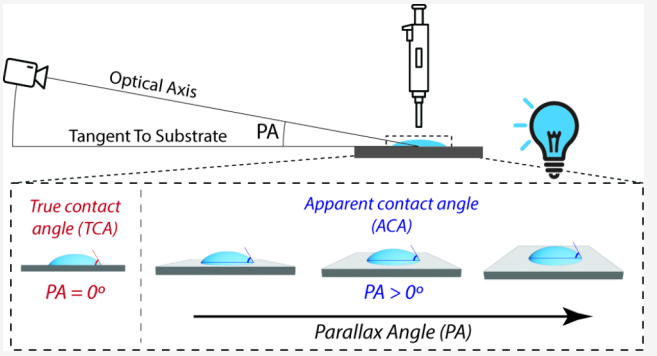

1. INTRODUCTION

Contact angle goniometry is one of the experimental methods available for quantitatively evaluating the surface energy of solids.[1] This has made it a vital tool for the development of a number of technologies across several science and engineering fields (e.g., materials science and engineering,[2] environmental science,[3] medicine,[4] petroleum engineering[5]), such as superhydrophobic coatings for aircraft wings[6] and processing methods for vaccines.[7] The process of performing a sessile drop contact angle measurement has greatly been simplified by the advent of commercially available, user-friendly, and multimodal instruments, which, for example, can automatically deposit arrays of liquid droplets onto a substrate, image the drops with a high-speed camera, and simultaneously analyze the images in a matter of seconds. These commercial instruments have a nominal contact angle accuracy as low as 0.1°.[8,9] Despite these remarkable advancements, the simple and automated nature of these measurements might result in users overlooking significant sources of experimental error, which can potentially cause misrepresentation of the results if only considering the instrument-reported accuracy or the random error from multiple, independent measurements.

Precisely measuring the wetting properties of surfaces that exhibit either very low (<10°) or high (>150°) contact angles using the sessile drop method is particularly challenging.[10,11] This is concerning because superhydrophobic and superhydrophilic materials and their wetting properties are widely studied, with active research areas in, for example, superhydrophobic textiles,[12−14] antifouling,[15−17] and anti-icing[18−20] surfaces. Given the plethora of research studies on these surfaces, it is important to identify sources of experimental

Received: November 28, 2023
Revised: January 25, 2024
Accepted: February 9, 2024
Published: February 26, 2024

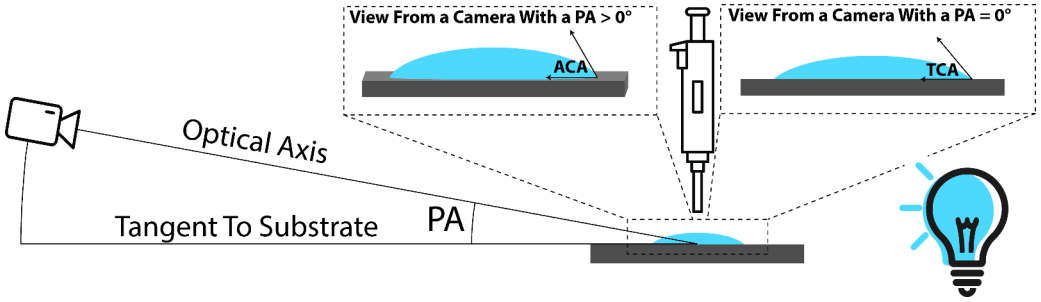

Figure 1. Schematic of a standard goniometer set up, consisting of a pipet that dispenses a sessile drop onto a substrate and an optical system made of a light source and an opposing high-speed CCD camera. The parallax angle (PA) is the angle between the optical axis of the camera and the substrate surface. Inset images show what the sessile drop looks like at different PAs. When the PA > 0°, the contact angle is the apparent contact angle (ACA). When the PA = 0°, the contact angle is the true contact angle (TCA).

error in goniometry measurements, as well as evaluate and report the magnitude of the resulting accuracy of the measurement. As one particular example, in the case of superhydrophobic surfaces it has been observed that, as the contact angle approaches 180°, the region of the three-phase contact, where the contact angle is measured, becomes difficult to properly resolve especially in cases of substrates that are not perfectly smooth, thus hindering the precise identification of the contact location and the point at which the contact angle should be measured.[21] This issue can lead to significant uncertainties in contact angles measured on superhydrophobic surfaces, as the computed contact angle strongly varies with even small variations in the height of the apparent three-phase contact. For example, one study on surfaces with a water contact angle (WCA) of 170° found that the magnitude of the contact angle error ranged from 1° up to 4° depending on the resolution of the drop image, with lower errors reported from higher resolution images.[10]

While improving the resolution of the imaging camera can alleviate issues related to identifying the location of the three-phase contact, another source of error in contact angle measurements, which is often overlooked, originates from the camera's parallax angle (PA). The PA, also called the camera's inclination, is the angle between the optical axis of the camera and the surface of the sample stage (in other words, the PA is the angle that is complementary to the one between the optical axis of the camera and the normal to the sample stage), as shown in Figure 1. Acquiring images of sessile drops at a nonzero PA allows for exploiting the reflection of the sessile drop on the substrate in the accurate identification of the location of the three-phase contact point (through what is known as the mirror method).[22] The PA required to properly detect the reflection is not large and, generally, a good reflection can be seen at PA as low as 1°. Despite this, the PA often goes unreported in literature and, since increasing the PA leads to more visible reflections, the use of PAs above 1° is not experimentally uncommon. Some commercial goniometers allow PAs as high as 4° to be achieved,[8,9] but the PA can likely be increased further with instrument modification.

The camera's PA can have a significant impact on the results of the contact angle measurement.[23,24] When viewed from a PA higher than 0°, the apparent profile of the drop differs from the true drop profile described by the Young−Laplace equation:[25,26]

$$-\gamma\left(\frac{1}{R_1}+\frac{1}{R_2}\right)=\Delta p \tag{1}$$

where γ is the liquid/vapor interfacial energy, R_1 and R_2 are the principal radii of curvature of the drop, and Δp is the change in pressure across the interface at that position. This change in profile for PA > 0° leads to an apparent contact angle (ACA) that differs from the true contact angle (TCA). The effect of a nonzero PA has been considered in the literature as several studies identified the PA as a possible source of systematic error, which can be minimized by capturing images at the lowest possible PA.[27−29] However, very little work has been carried out to quantify the error in contact angle measurements as a function of the PA. While few research articles have looked at the magnitude of the error in contact angle due to a nonzero PA, these investigations have been limited and relied on geometric assumptions.[23,24] For instance, Sobolev and Brugnara approximated the shape of the drop on a flat surface as a spherical cap instead of using eq 1.[23,24] Under this geometric assumption, an equation for computing the ACA from the height of the drop (h) and its radius (r) was derived:

$$\tan\left(\frac{\mathrm{ACA}}{2}\right)=\frac{h}{r} \tag{2}$$

The ACA was then geometrically related to the PA through the following equation:

$$\tan\left(\frac{\mathrm{ACA}}{2}\right)=\frac{1-\cos(\mathrm{TCA})\cos(\mathrm{PA})}{\sin(\mathrm{TCA})} \tag{3}$$

Eq 3 thus allows for the quantification of the TCA once the ACA and PA are computed (eq 2) or known. However, the spherical cap approximation underpinning the equations derived by Sobolev and Brugnara is only valid when drops are small enough that gravity does not have a large effect on their shape.[23,24] Despite the relevance of the results, the study only investigated the effect of a finite PA on TCAs up to 110° and did not consider TCAs > 150° (i.e., superhydrophobic surfaces) or TCAs < 10° (i.e., superhydrophilic surfaces). The outcomes of the works by Sobolev and Brugnara clearly indicated that significant errors in contact angle measurements can originate from nonzero PAs used in goniometry measurements, while also suggesting that more in-depth investigations of their magnitude are needed, especially in cases where the spherical approximation does not hold and in the case of superhydrophobic/superhydrophilic surfaces.

It has to be highlighted that an in-depth study of the errors in contact angle measurements due to finite PAs over a large range of TCAs is difficult for two main reasons. First, experimentally studying the magnitude of the errors over a wide range of TCAs requires identifying solid/liquid

https://doi.org/10.1021/acs.langmuir.3c03684
Langmuir 2024, 40, 5090−5097

combinations with the desired interfacial energies. Second, experimental challenges in accurately positioning the camera must also be considered, as the camera's position (both horizontal and vertical) needs to change to vary the PA such that the focal distance to the sessile drop and the drop's position in the image do not vary. Finally, it must be underlined that under normal experimental conditions, other sources of error can affect contact angle measurements, including the effect of contact line obscuration outlined above, and the temporal evolution of sessile drop shape during observations due to, for example, evaporation. Thus, any experimental efforts focusing on the evaluation of the effect of the PA on the accuracy of contact angle measurements should carefully rule out or quantify other sources of uncertainty in the measurements.

To circumvent these experimental difficulties, in the present work virtual contact angle measurements were carried out by creating synthetic sessile drops using the Young−Laplace equation (eq 1) and imaging them using a virtual camera. The results of the drop analysis, performed using the axisymmetric drop shape analysis (ADSA) method, allow for the quantification of the magnitude of the errors in contact angle (for TCAs ranging from 5° (superhydrophilic) to 175° (superhydrophobic)) due to PAs up to 10°. The effect of the droplet geometry on the error was also be investigated. The outcomes of this work do not only provide guidelines to experimentalists for minimizing systematic errors in contact angle measurements due to the finite PA employed in experimental instruments, but also demonstrates the significance of the errors introduced in contact angle measurements due to nonzero PAs especially when dealing with superhydrophilic/superhydrophobic surfaces. Finally, the results of this study highlight the importance of reporting the PA in experimental sections of the published literature.

2. METHODS

2.1. Creating Virtual Sessile Drops. Virtual sessile drops were created in MATLAB R2022a using a system of differential equations derived from eq 1 as described by Hoofar and Neumann:[30]

$$\frac{dx}{ds} = \cos(\varphi) \tag{4}$$

$$\frac{dz}{ds} = \sin(\varphi) \tag{5}$$

$$\frac{d\varphi}{ds} = 2b + cz - \frac{\sin(\varphi)}{x} \tag{6}$$

where (x,z) are the horizontal and vertical Cartesian coordinates of the sessile drop profile, s is the arc length from the apex of the drop to (x,z), φ is the angle between the tangent at (x,z), and the x-axis as shown in Figure 2.

The constants b and c define the shape of the drop and are usually called the shape parameters as b is the curvature at the apex of the drop (i.e., the inverse of the radius of curvature R_0, shown in Figure 2) and c is the capillary constant of the liquid phase, which is given by

$$c = \frac{(\Delta\rho)g}{\gamma} \tag{7}$$

where $\Delta\rho$ is the density difference across the liquid/gas interface, g is the acceleration due to gravity (9.81 m s^{-2}), and γ is the energy of the liquid/gas interface.

In this study, water under ambient conditions (25 °C, 1 atm, 65% RH) is considered, as it is the most studied liquid in sessile drop experiments. In this case, the capillary constant c is equal to 13.45 cm^{-2}.[31] The apex curvature, b, depends on the solid substrate material as well as the volume of the sessile drop. For this study, three values of b, namely 1 cm^{-1}, 5 cm^{-1}, and 10 cm^{-1}, were considered. These values were selected as they cover a wide range of volumes at each true contact angle (TCA) and are similar to the values presented by Del Rio.[31]

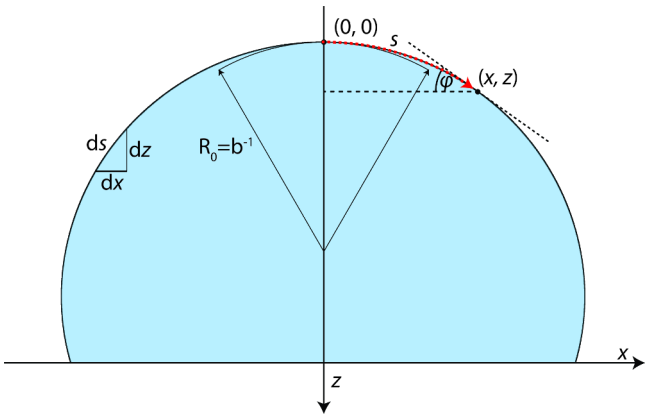

Figure 2. Virtual sessile drop variables involved in the Young−Laplace system of ordinary differential equations. (x, z) are the spatial coordinates of the sessile drop's edge; (0, 0) is set as the apex of the drop. s is the arc length from the drop's apex to the (x, z) point; φ is the angle between the x-axis and the tangent at (x, z).

The following Dirichlet boundary conditions were used to solve eqs 4−6:

$$x(0) = 0 \rightarrow z(0) = \varphi(0) = 0 \tag{8}$$

with the point (0, 0) being the apex of the drop profile. At $x = 0$, eq 6 is undefined. However, since

$$\lim_{s,x,\varphi\rightarrow 0} \frac{\sin(\varphi)}{x} = b \tag{9}$$

Eq 6 can be rewritten as[30]

$$\frac{d\varphi}{ds} = b \tag{10}$$

For any given b and c values, eqs 4−6, and its associated boundary conditions (eq 8−9), are numerically solved using the ODE45 function in MATLAB to produce sessile drop profiles. An example of sessile drop profile is shown in Figure 3a. In the present work, the height of the drop's base is systematically changed to obtain drops with different contact angles (ranging from 5° (superhydrophilic) to 175° (superhydrophobic)). The dashed lines in Figure 3a give an example of the effect of changing the height of the drop and the resulting contact angles. The sessile drop profiles, along with their vertically mirrored images, are then converted to a 3-dimensional drop, shown in Figure 3b, by revolving the profile around the z axis.

To assist with the conversion of the coordinates from pixels to centimeters, 4 calibration spheres of known size are placed around the drop as shown in Figure 3c. To average out any errors that might arise as a result of the calibration process (see section 2.2) and any dependency on the size of the calibration sphere, 6 images, each with different calibration sphere sizes, were created. The 6 calibration sphere diameters were equal to the height of a drop with a 180° TCA multiplied by a scaling factor (0.2, 0.25, 0.3, 0.35, 0.4, and 0.45).

Finally, the parallax angle (PA) of the camera is incrementally changed from 0° to 10°, covering an angular range that is normally allowed in experimental goniometers. At each PA, a high-resolution (3000 ppi) image of the drop is acquired. Figure 3d shows the same drop shown in Figure 3c but viewed from a PA of 10°. While Figure 3d looks similar to Figure 3c, the drop's end points are rounded. More information about the creation and imaging procedures of virtual drops is provided in the Supporting Information.

https://doi.org/10.1021/acs.langmuir.3c03684
Langmuir 2024, 40, 5090−5097

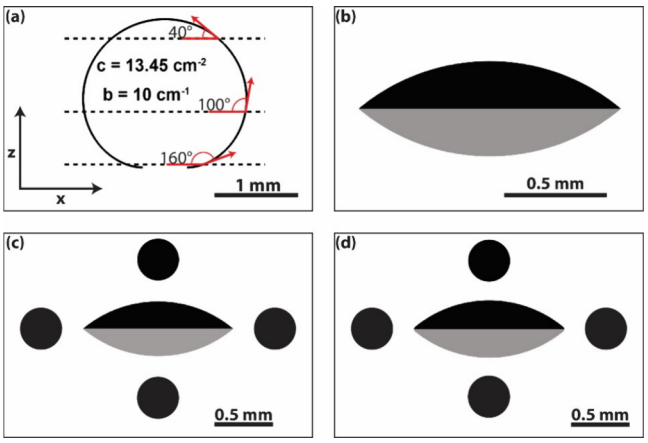

Figure 3. Procedure for creating a virtual sessile drop. (a) Drop profile based on the numerical solution to the Young−Laplace equation with known b and c values. The height of the virtual surface is systematically changed to obtain profiles with different contact angles. (b) Example of drop profile together with its vertical reflection (shaded gray). The profile is transformed into a surface plot, i.e., a 3D sessile drop, by revolving it around the z axis. (c) Calibration spheres, with diameters equal to the height of a 180° TCA drop multiplied by 0.2, are placed around the sessile drop to help with the conversion of pixel coordinates to coordinates in cm. (d) Drop profile generated in (c), but viewed PA of 10°.

2.2. Analyzing Virtual Sessile Drops. To determine the apparent contact angle (ACA), virtual sessile drops were analyzed in MATLAB using a MATLAB-based axisymmetric drop shape analysis (ADSA) program similar to those found in literature.[30−33] First, a canny edge detection method is used to extract the drop's profile in the form of pixel coordinates, (x, z), of the sessile drop's edge.[34] The top half of the extracted profile is then isolated from the reflection using the known contact line. The arc length s (from the apex of the drop to each (x, z) point along the profile) is found using a digital arc length finder based on the minimum length polygon method.[35] The extracted (x, z, s) coordinates are converted from pixels to centimeters using a scaling factor calculated from the calibration spheres. An optimization method is used to determine the drop shape constants (b and c) from the best fit (using eqs 4−6) of the drop profile. The optimized best-fit profile is then used to calculate the virtual drop's ACA. This ADSA method is done independently for 6 images of each sessile drop, each with different calibration sphere sizes, and the results at each PA are averaged. The error in the results introduced by the ADSA method is taken to be the average difference between the TCA and the ACA at PA equal to 0° and found to be between 0.1° and 0.5° depending on the TCA and b value. A more in-depth explanation of the steps in the drop analysis is provided in the Supporting Information.

3. RESULTS AND DISCUSSION

To determine the error in contact angle measurements due to the camera angular positioning (i.e., PA) for sessile drops with various true contact angles (TCAs), virtual sessile drop experiments were performed. Figure 4 shows the absolute (Figure 4a) and relative (Figure 4b) contact angle error for sessile drops created with an apex curvature of 1 cm^{-1} (similar plots for drops with an apex curvature of 5 and 10 cm^{-1} are provided in the Supporting Information, Figures S.3−S.6). Increasing the PA for drops having TCAs lower than 90° results in an overestimation of the contact angle (i.e., positive absolute error), while in the case of drops with TCAs above 90° the contact angle is underestimated upon increasing the PA (i.e., negative absolute error) (Figure 4a). Notably, the

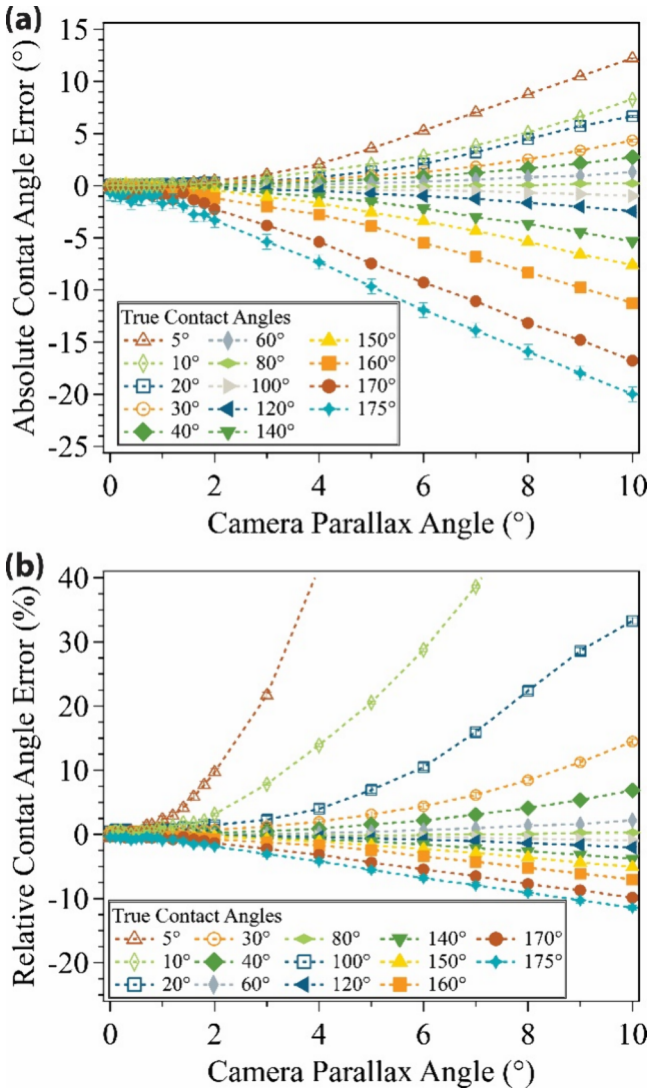

Figure 4. (a) Absolute error (i.e., difference between the apparent contact angle (ACA, θ_a) and true contact angle (TCA, θ_c)) and (b) relative error (i.e., $(\theta_a - \theta_c)/\theta_c \times 100$) in contact angle measurements for drops with TCAs ranging from 5° to 175°. The virtual drops have an apex curvature value (b value in eq 6) of 1 cm^{-1} and were imaged at camera PAs up to 10°.

magnitude of the absolute contact angle error increases as the TCA deviates from 90° and reaches a value of 12.2° and −20° for TCA equal to, respectively, 5° and 175° at the highest PA considered in this work (i.e., 10°). These values correspond to relative errors of 245% and −11%, respectively, thus highlighting the significant effect of the PA on the accurate quantification of the contact angle.

Since the uncertainty in contact angle measurements (usually computed from multiple independent measurements, meaning that this is the random error in the measurements) is commonly reported to be ±1°−2°,[36] the PA value required to have an absolute, systematic error greater than +1° (for TCA < 90°) or smaller than −1° (for TCA > 90°) was estimated based on the data reported in Figure 4 and plotted as a function of the TCA in Figure 5. While the PA needed to induce an absolute contact angle error greater than +1° (for TCA < 90°) or smaller than −1° (for TCA > 90°) is large for TCA close to 90°, it rapidly decreases as the TCA deviates from 90° and reaches values smaller than 5° for TCA below

https://doi.org/10.1021/acs.langmuir.3c03684
Langmuir 2024, 40, 5090−5097

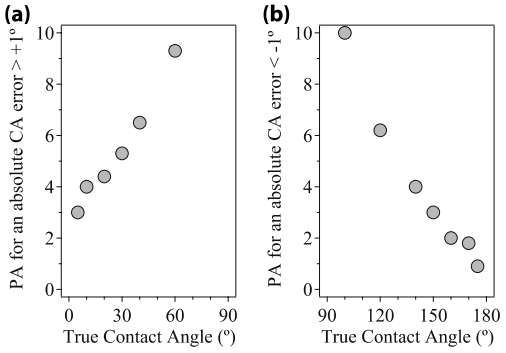

Figure 5. Parallax angle (PA) required for achieving an absolute contact angle (CA) error greater than +1° for TCA below 90° (a) or smaller than −1° for TCA above 90° (b) as a function of the TCA. The virtual drops have an apex curvature value (b value in eq 6) of 1 cm^{-1}.

30° or above 140°. Notably, these results indicate that in the case of superhydrophobic and superhydrophilic surfaces, extremely small angular rotations of the optical axis of the imaging camera (e.g., a PA equal to 1° for a drop having a TCA of 175°) leads to absolute, systematic errors in contact angle measurements exceeding 1°.

Figure 6 provides a visual representation of the effect of changing the PA of the optical camera on the imaged drop shape for TCA equal to 20°, 90°, and 160°. As the PA increases, the shape of the drop section above the contact line (the darker section) changes and become more circular. For drops with TCAs of 20° and 160°, this change in shape is more significant than it is for the drop with a TCA of 90°, thus resulting in larger changes in the apparent contact angle (ACA). This results in larger absolute and relative errors as shown in Figure 4.

Altogether, these results indicate that significant errors in contact angle measurements are introduced by the acquisition of optical images of sessile drops at a finite, nonzero PA. Additionally, the magnitude of these systematic errors exceeds the experimental uncertainty normally reported in the literature for contact angle measurements.[37−39] This finding not only highlights the importance of considering the PA when interpreting the outcomes of sessile drop measurements, but also underlines the necessity of reporting the PA in experimental sections of the published literature.

The magnitude of the absolute error induced by the nonzero PA is not only dependent on the TCA, but also shows a strong dependency on the drop shape, and, in particular, the curvature of the drop apex (b). Figure 7 shows the absolute contact angle

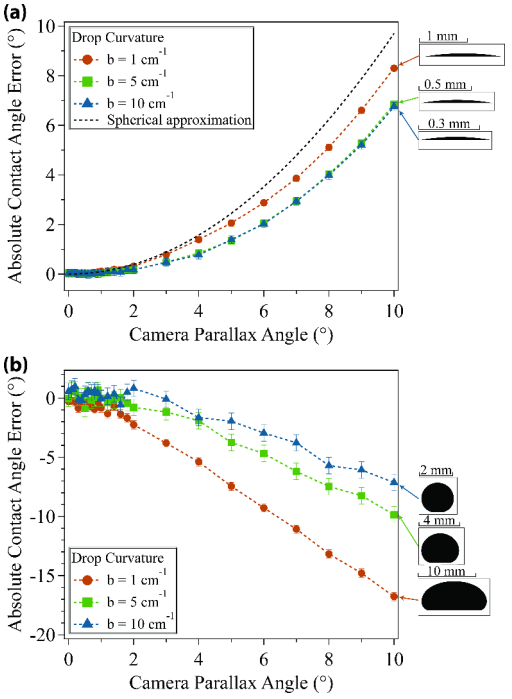

Figure 7. Effect of the shape drop (curvature of the drop apex b) on the absolute error in contact angle measurements. Absolute error in contact angle as a function of PA for drops with a TCA of 10° (a) and 170° (b) and with three different values of apex curvature (1 cm^{-1}, 5 cm^{-1}, and 10 cm^{-1}). The images on the side of the graph show the drop shape at a PA of 0°. The dashed black line in (a) corresponds to the dependence of the ACA on the PA predicted by the spherical cap approximation (eq 3).[23]

error for drops with apex curvature of 1 cm^{-1}, 5 cm^{-1}, and 10 cm^{-1} and TCA equal to 10° (Figure 7a) and 170° (Figure 7b). As the apex curvature of the drop increases (i.e., upon

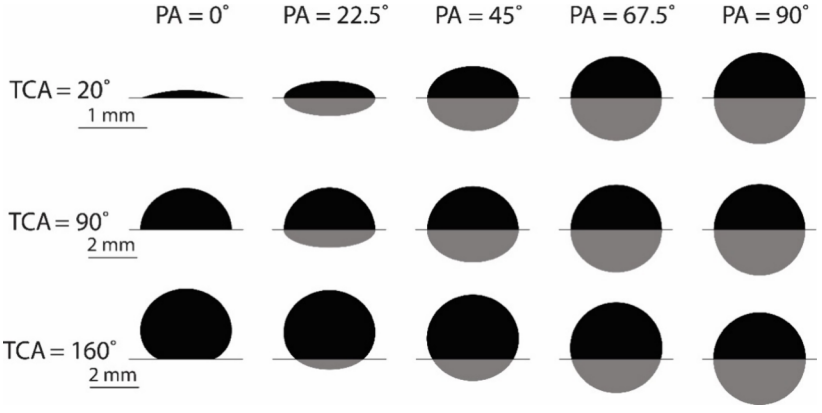

Figure 6. Effect of extreme PAs on sessile drops with TCAs of 20°, 90°, and 160°. The dark regions of the drops are the sections above the baseline and, thus, the sections that would be used to calculate the ACA. As the PA increases, the dark sections of the drops with TCAs of 20° and 160° significantly change in shape, while the dark section of the drop with a TCA of 90° does not vary. This illustrates that the more the TCA deviates from 90°, the larger the impact of parallax errors on the measured ACAs.

https://doi.org/10.1021/acs.langmuir.3c03684
Langmuir 2024, 40, 5090−5097

increasing b), the absolute value of the error decreases at any PA. As a particular example, the errors for drops with TCA of 10° and imaged at a PA of 10° are 8.3°, 6.9°, and 6.8° for curvatures of 1 cm^{-1}, 5 cm^{-1}, and 10 cm^{-1}, respectively. Similar results were observed for high TCAs: in the case of a drop with TCA equal to 170°, the absolute error decreases from 16.7° to 6.5° upon increasing the apex curvature from 1 to 10 cm^{-1} (at PA = 10°).

The outcomes of this study, highlighting the magnitude of the errors introduced in the estimation of the contact angle by the acquisition of optical images at nonzero PAs, call for the development of methods that would enable the computation of the TCA once the ACA is measured and the PA is experimentally determined. As pointed out in the introduction, Sobolev proposed a method for calculating the TCA from measured ACA values at a fixed PA (eq 3).[23] As indicated by the solid black line in Figure 7a, the model does not accurately describe errors in contact angle measurements when the ADSA is used in place of the spherical cap approximation. One of the issues when using eq 3 to compute deviations in contact angle when drops are imaged at nonzero PA is that it does not consider the curvature of the drop, which has been shown to have a significant impact on the magnitude of parallax errors. This result highlights that, when using the ADSA, any relationship relating the PA and ACA to the TCA must take the drop shape (i.e., apex curvature b) into account.

The development of a geometric function, similar to the one in eq 3, relating contact angle error to the PA when utilizing the ADSA is exceedingly difficult and beyond the scope of this work. The challenges associated with the derivation of an analytical expression for computing TCAs from measured ACAs at known PAs originate from the complexity of the drop shape, which is described by a system of three differential equations (eqs 4−6). Furthermore, even in the case that the apparent 2-D drop profile can be computed at any given (nonzero) PA, fitting it with eq 4−6 would still be difficult as it is not a true sessile drop shape described by the Young−Laplace equation. Further work needs to be carried out on the topic and will be part of a separate study.

4. PRACTICAL GUIDELINES

In the absence of a geometrically derived function relating the APA to the PA, one reliable way to reduce errors when using the axisymmetric drop shape analysis is to minimize the PA during collection of drop images. For the three drop shapes discussed in this study (with apex curvatures of 1 cm^{-1}, 5 cm^{-1}, and 10 cm^{-1}), a PA of 1° would result in absolute, systematic errors in the measured contact angle that are either smaller than +1° for TCA < 90° or greater than −1° for TCA > 90° (Figure 5). However, reducing the PA might lead to challenges for the unambiguous identification of the contact line. In cases in which lowering the PA below 1−2° is not feasible, reducing the size of the sessile drop is an effective way to decrease the error in contact angle measurements as it will increase the curvature of the drop apex while theoretically keeping the TCA constant.[40] Figure 7b displays sessile drops having the same TCA (170°) but different volumes (381 μL, 23 μL, and 4 μL), which result in different apex curvature (1 cm^{-1}, 5 cm^{-1}, and 10 cm^{-1}, respectively). Upon considering a fixed PA, decreasing the volume of the drop drastically reduces the absolute error in the measured contact angle. It has to be highlighted that, even though reducing the drop volume would allow decreasing errors in contact angle due to the acquisition of drop images at finite PAs, lowering the liquid volume could potentially result in an increase in the uncertainty of the measurements due to other sources of errors, such as optical metrology errors,[41] and effects of surface heterogeneity.[42]

5. CONCLUSIONS

The magnitude of the error in contact angle measurements caused by imaging sessile drops at nonzero parallax angles (PAs) has been quantitatively evaluated using synthetic drops defined by the Young−Laplace equation. The absolute error increases as the true contact angle (TCA) deviates from 90° and results in an overestimation (underestimation) of the contact angle for drops having TCAs lower (higher) than 90°. The computed absolute error reaches values as high as −20° (12.2°) for drops having a TCA of 175° (5°) when imaged with a PA of 10°, thus indicating the importance of considering the PA when accurately quantifying contact angles in sessile drop experiments. Changing the apex curvature of the sessile drops also has an impact on the magnitude of the absolute error induced by the collection of drop images at nonzero PAs. In particular, drops with higher apex curvatures exhibited lower absolute error than those with lower curvatures at any given PA. The comparison between the computed absolute error with a spherical approximation-based model describing the evolution of the drop shape with the PA indicated that the model does not accurately describe errors in contact angle measurements when the drops are fit with the axisymmetric drop shape analysis (ADSA) method. Further work is required to develop an analytical expression that correlates the apparent contact angle measured at a given PA to the TCA. Altogether, the present work provides guidelines for minimizing errors in sessile drop measurements due to the finite PA. First, decreasing the PA allows for minimizing the absolute errors in contact angle measurements even in the case of superhydrophobic and superhydrophilic surfaces. Second, reducing the size of the sessile drop can decrease the error in contact angle measurements as it will increase the curvature of the drop apex. In summary, the outcomes of this work can help scientists and engineers increase the accuracy of sessile drop measurements by minimizing errors induced by the acquisition of drop images at finite PAs.

■ ASSOCIATED CONTENT

Supporting Information

The Supporting Information is available free of charge at https://pubs.acs.org/doi/10.1021/acs.langmuir.3c03684.

Description of the method for creating and imaging sessile drops; procedure for analyzing the shape of sessile drops; absolute and relative contact angle error for sessile drops created with an apex curvature of 5 and 10 cm^{-1} (PDF)

■ AUTHOR INFORMATION

Corresponding Author

Filippo Mangolini − *Walker Department of Mechanical Engineering, The University of Texas at Austin, Austin, Texas 78712, United States; Texas Materials Institute, The University of Texas at Austin, Austin, Texas 78712, United States;* orcid.org/0000-0003-3360-9122; Email: Filippo.Mangolini@austin.utexas.edu

https://doi.org/10.1021/acs.langmuir.3c03684
Langmuir 2024, 40, 5090−5097

Author

Owen M. Johnson − *Walker Department of Mechanical Engineering, The University of Texas at Austin, Austin, Texas 78712, United States*

Complete contact information is available at: https://pubs.acs.org/10.1021/acs.langmuir.3c03684

Author Contributions

Owen Johnson: Conceptualization, methodology, software, formal analysis, writing - original draft. Filippo Mangolini: Conceptualization, supervision, writing - original draft, funding acquisition.

Notes

The authors declare no competing financial interest.

■ ACKNOWLEDGMENTS

The material is based upon work supported by the Welch Foundation (Grant No. F-2151-20230405) and the National Science Foundation Faculty Early Career Development Program (Grant No. 2042304). Last, but not least, this paper is dedicated to Prof. em. Nicholas D. Spencer, whose guidance, mentorship, and continuous support uniquely contributed to the development of the next-generation of scientists and engineers and whose generous leadership in the surface science and tribology communities will be inspirational for the generations to come.

■ ABBREVIATIONS

ACA, apparent contact angle; ADSA, axisymmetric drop shape analysis; TCA, true contact angle; PA, parallax angle

■ REFERENCES

(1) Zisman, W. A. Relation of the Equilibrium Contact Angle to Liquid and Solid Constitution. *Contact Angle, Wettability, and Adhesion* **1964**, *43*, 1−51.

(2) Bai, Y.; Zhang, H.; Shao, Y.; Zhang, H.; Zhu, J. Recent Progresses of Superhydrophobic Coatings in Different Application Fields: An Overview. *Coatings 2021, Vol. 11, Page 116* **2021**, *11* (2), 116.

(3) Wang, H.; Shi, H.; Li, Y.; Yu, Y.; Zhang, J. Seasonal Variations in Leaf Capturing of Particulate Matter, Surface Wettability and Micromorphology in Urban Tree Species. *Front. Environ. Sci. Eng.* **2013**, *7*, 579.

(4) Muster, T. H.; Prestidge, C. A. Water Adsorption Kinetics and Contact Angles of Pharmaceutical Powders. *Journal of Pharmaceutical Sciences* **2005**, *94*, 861.

(5) Dos Santos, R. G.; Mohamed, R. S.; Bannwart, A. C.; Loh, W. Contact Angle Measurements and Wetting Behavior of Inner Surfaces of Pipelines Exposed to Heavy Crude Oil and Water. *Journal of Petroleum Science and Engineering* **2006**, *51*, 9.

(6) Piscitelli, F.; Chiariello, A.; Dabkowski, D.; Corraro, G.; Marra, F.; Di Palma, L. Superhydrophobic Coatings as Anti-Icing Systems for Small Aircraft. *Aerospace 2020, Vol. 7, Page 2* **2020**, *7* (1), 2.

(7) Dao, H. M.; Sahakijpijarn, S.; Chrostowski, R.; Peng, H.-H.; Moon, C.; Xu, H.; Mangolini, F.; Do, H. H.; Cui, Z.; Williams, R. O. Entrapment of Air Microbubbles by Ice Crystals during Freezing Exacerbates Freeze-Induced Denaturation of Proteins. *Int. J. Pharm.* **2022**, *628*, 122306.

(8) Biolin Scientific. *Theta Flex | Attension | Optical Tensiometers*. https://www.biolinscientific.com/attension/optical-tensiometers/theta-flex#specifications (accessed 2023-11-13).

(9) KRÜSS Scientific. *Drop Shape Analyzer-DSA100E*. https://www.kruss-scientific.com/en-US/products-services/products/dsa100e (accessed 2023-11-13).

(10) Vuckovac, M.; Latikka, M.; Liu, K.; Huhtamäki, T.; Ras, R. H. A. Uncertainties in Contact Angle Goniometry. *Soft Matter* **2019**, *15* (35), 7089−7096.

(11) Nagy, N. Contact Angle Determination on Hydrophilic and Superhydrophilic Surfaces by Using R-?-Type Capillary Bridges. *Langmuir* **2019**, *35* (15), 5202−5212.

(12) Ahmad, I.; Kan, C. W. A Review on Development and Applications of Bio-Inspired Superhydrophobic Textiles. *Materials 2016, Vol. 9, Page 892* **2016**, *9* (11), 892.

(13) Park, S.; Kim, J.; Park, C. H. Superhydrophobic Textiles: Review of Theoretical Definitions, Fabrication and Functional Evaluation. *Journal of Engineered Fibers and Fabrics* **2015**, *10* (4), No. 155892501501000.

(14) Zimmermann, J.; Reifler, F. A.; Fortunato, G.; Gerhardt, L. C.; Seeger, S. A Simple, One-Step Approach to Durable and Robust Superhydrophobic Textiles. *Adv. Funct Mater.* **2008**, *18* (22), 3662−3669.

(15) Chapman, J.; Regan, F. Nanofunctionalized Superhydrophobic Antifouling Coatings for Environmental Sensor Applications—Advancing Deployment with Answers from Nature. *Adv. Eng. Mater.* **2012**, *14* (4), B175−B184.

(16) Chung, J. S.; Kim, B. G.; Shim, S.; Kim, S. E.; Sohn, E. H.; Yoon, J.; Lee, J. C. Silver-Perfluorodecanethiolate Complexes Having Superhydrophobic, Antifouling, Antibacterial Properties. *J. Colloid Interface Sci.* **2012**, *366* (1), 64−69.

(17) Xue, C.-H.; Guo, X.-J.; Ma, J.-Z.; Jia, S.-T. Fabrication of Robust and Antifouling Superhydrophobic Surfaces via Surface-Initiated Atom Transfer Radical Polymerization. *ACS Appl. Mater. Interfaces* **2015**, *7*, 8251.

(18) Cao, L.; Jones, A. K.; Sikka, V. K.; Wu, J.; Gao, D. Anti-Icing Superhydrophobic Coatings. *Langmuir* **2009**, *25* (21), 12444−12448.

(19) Farhadi, S.; Farzaneh, M.; Kulinich, S. A. Anti-Icing Performance of Superhydrophobic Surfaces. *Appl. Surf. Sci.* **2011**, *257*, 6264−6269.

(20) Li, W.; Zhan, Y.; Yu, S. Applications of Superhydrophobic Coatings in Anti-Icing: Theory, Mechanisms, Impact Factors, Challenges and Perspectives. *Prog. Org. Coat.* **2021**, *152*, 106117.

(21) Dorrer, C.; Ruhe, J. Advancing and Receding Motion of Droplets on Ultrahydrophobic Post Surfaces. *Langmuir* **2006**, *22* (18), 7652−7657.

(22) Saulick, Y.; Lourenço, S. D. N.; Baudet, B. A. A Semi-Automated Technique for Repeatable and Reproducible Contact Angle Measurements in Granular Materials Using the Sessile Drop Method. *Soil Science Society of America Journal* **2017**, *81* (2), 241−249.

(23) Sobolev, V. D.; Starov, V. M.; Velarde, M. G. On the Accuracy of Measuring Small Contact Angles by the Sessile Drop Method. *Colloid Journal of the Russian Academy of Sciences: Kolloidnyi Zhurnal* **2003**, *65* (5), 611−614.

(24) Brugnara, M.; Volpe, C. D.; Siboni, S.; Zeni, D. Contact Angle Analysis on Polymethylmethacrylate and Commercial Wax by Using an Environmental Scanning Electron Microscope. *Scanning* **2006**, *28* (5), 267−273.

(25) Young, T. An Essay on the Cohesion of Fluids. *Abstracts of the Papers Printed in the Philosophical Transactions of the Royal Society of London* **1832**, *1*, 171−172.

(26) Laplace, P. S. *Traité de Mécanique Céleste* **1798**, DOI: 10.5479/SIL.338664.39088005644752.

(27) Chinnam, J.; Das, D.; Vajjha, R.; Satti, J. Measurements of the Contact Angle of Nanofluids and Development of a New Correlation. *International Communications in Heat and Mass Transfer* **2015**, *62*, 1−12.

(28) Kalantarian, A.; David, R.; Neumann, A. W. Methodology for High Accuracy Contact Angle Measurement. *Langmuir* **2009**, *25* (24), 14146−14154.

(29) Huhtamäki, T.; Tian, X.; Korhonen, J. T.; Ras, R. H. A. Surface-Wetting Characterization Using Contact-Angle Measurements. *Nature Protocols 2018 13:7* **2018**, *13* (7), 1521−1538.

(30) Hoorfar, M.; Neumann, A. W. Recent Progress in Axisymmetric Drop Shape Analysis (ADSA). *Adv. Colloid Interface Sci.* **2006**, *121* (1−3), 25−49.
(31) Del Río, O. I.; Neumann, A. W. Axisymmetric Drop Shape Analysis: Computational Methods for the Measurement of Interfacial Properties from the Shape and Dimensions of Pendant and Sessile Drops. *J. Colloid Interface Sci.* **1997**, *196* (2), 136−147.
(32) Saad, S. M. I.; Neumann, A. W. Axisymmetric Drop Shape Analysis (ADSA): An Outline. *Adv. Colloid Interface Sci.* **2016**, *238*, 62−87.
(33) Hoorfar, M.; Neumann, A. W. Axisymmetric Drop Shape Analysis (ADSA) for the Determination of Surface Tension and Contact Angle. *J. Adhes* **2004**, *80* (8), 727−743.
(34) Canny, J. F. *Finding Edges and Lines in Images*, 1983. https://dspace.mit.edu/handle/1721.1/6939 (accessed 2023-11-13).
(35) Klette, R.; Rosenfeld, A. *Digital Geometry: Geometric Methods for Digital Picture Analysis*; Morgan Kaufmann, 2004.
(36) Johnson, R. E. Wettability and Contact Angles. *Surface and Colloid Science* **1969**, *2*, 85.
(37) Teare, D. O. H.; Spanos, C. G.; Ridley, P.; Kinmond, E. J.; Roucoules, V.; Badyal, J. P. S.; Brewer, S. A.; Coulson, S.; Willis, C. Pulsed Plasma Deposition of Super-Hydrophobic Nanospheres. *Chem. Mater.* **2002**, *14* (11), 4566−4571.
(38) Wang, B.-B.; Zhao, Y.-P.; Yu, T. Fabrication of Novel Superhydrophobic Surfaces and Droplet Bouncing Behavior — Part 2: Water Droplet Impact Experiment on Superhydrophobic Surfaces Constructed Using ZnO Nanoparticles. *J. Adhes Sci. Technol.* **2011**, *25* (1−3), 93−108.
(39) Guo, Z. G.; Fang, J.; Hao, J. C.; Liang, Y. M.; Liu, W. M. A Novel Approach to Stable Superhydrophobic Surfaces. *ChemPhysChem* **2006**, *7* (8), 1674−1677.
(40) Extrand, C. W.; Moon, S. I. When Sessile Drops Are No Longer Small: Transitions from Spherical to Fully Flattened. *Langmuir* **2010**, *26* (14), 11815−11822.
(41) Srinivasan, S.; McKinley, G. H.; Cohen, R. E. Assessing the Accuracy of Contact Angle Measurements for Sessile Drops on Liquid-Repellent Surfaces. *Langmuir* **2011**, *27* (22), 13582−13589.
(42) Drelich, J. The Effect of Drop (Bubble) Size on Contact Angle at Solid Surfaces. *J. Adhes* **1997**, *63* (1−3), 31−51.

https://doi.org/10.1021/acs.langmuir.3c03684
Langmuir 2024, 40, 5090−5097